20

Modern biophotonics methods as a powerful practice on dosage regime determination illustrated by endovascular administration of polymer microcapsules during targeted delivery

© O.I. Gusliakova[1,2], E.S. Prikhozhdenko[2], V.O. Plastun[2], O.A. Mayorova[2], N.A. Shushunova[2], O.A. Kulikov[3], A.S. Abdurashitov[1], D.A. Gorin[4], G.B. Sukhorukov[1,5], O.A. Sindeeva[1]

[1] Vladimir Zelman Center for Neurobiology and Neurorehabilitation, Skolkovo Institute of Science and Technology, 121205 Moscow, Russia
[2] Scientific Medical Center, Saratov State University, 410012 Saratov, Russia
[3] Institute of Medicine, National Research Mordovian State University named after Ogarev, 430005 Saransk, Russia
[4] Center for Photonics and Quantum Materials, Skolkovo Institute of Science and Technology, 121205 Moscow, Russia
[5] Life Improvement by Future Technologies Center, 143025 Skolkovo, Moscow, Russia

e-mail: O.Gusliakova@skoltech.ru, O.Sindeeva@skoltech.ru

Received December 20, 2023
Revised February 27, 2024
Accepted March 05, 2024

Rational selection of dosage regimen is the key to the future success of the therapeutic effectiveness of new therapeutic formulation. Modern visualization systems make it possible to in situ evaluate the effectiveness of selected parameters for carriers administrated into a living organism and make reasonable adjustments. In an effort to maximize the accumulation of drug delivery systems in the target organ during targeted delivery, one should not forget about maintaining normal physiological processes. The strategy of tandem use of imaging systems that evaluate the biodistribution of a certain fluorescent label and the state of individual organs or systems can speed up and simplify the process of selecting methods for conducting in vivo experiments. This article shows how assessing the biodistribution of a fluorescent conjugate associated with microcapsules using fluorescence tomography helps determine a dosage regimen for intra-arterial administration that ensures effective accumulation of carriers in the target mouse kidney, and a laser speckle-contrast imaging system allows us to eliminate dosages leading to the development of pathological conditions in the target organ.

Keywords: fluorescence, intravital imaging, biodistribution, laser speckle contrast imaging, microcapsules.

DOI: 10.61011/EOS.2024.03.58747.31-24

Introduction

The success of therapy depends on the correct choice of both the drug and the dosage regimen. The dosage regimen is a broad concept that covers the dose, the dosing interval, the duration of treatment, the pharmaceutical form, and the route of administration into the body [1]. The development of a new pharmaceutical form or therapeutic strategy necessarily requires selection or adjustment of the dosage regimen [2,3]. This is especially important in the context of testing the developed approaches on animals or transferring the results of animal testing into actual clinical practice [4,5]. Selection of a dosage regimen is also a prerequisite for correct and comprehensive testing of the behavior of new encapsulated forms of drugs, which enable their prolonged or controlled release, in the body. This requires the use of reliable and informative methods for analyzing the effect of developed pharmaceutical forms on individual organs and systems *in vivo*. The synergistic development of biophotonics and technology has led to the emergence of modern imaging systems that allow one to study the processes of interaction of the body with various external and internal factors, evaluate pharmacodynamics and the condition of tissues and organs, select diagnostic criteria, and diagnose diseases.

Fluorescence tomography is rightfully regarded as one of the systems of this kind. This method makes it possible to study non-invasively the biodistribution and accumulation of drugs (bound to a fluorescent label) in organs [6–8]. However, owing to the intense scattering and absorption of light by tissues, the detection depth of fluorophores in living objects is limited to several hundred micrometers. Therefore, the accumulation of a fluorescent signal may be studied only in the near-surface organs of small laboratory animals. Intense autofluorescence of body tissues is another significant problem [9]. Both these problems may be resolved in part through the use of near/mid-infrared illumination sources and the corresponding fluorophores [9]. Optical clearing agents may also increase the detection

depth of fluorescence tomography by reducing the light scattering coefficient temporarily [10].

Laser speckle contrast imaging (LSCI) is a promising tool for non-contact monitoring of blood and lymph flow in tissues [11,12]. It has also proven itself efficient in assessing the safety of encapsulated drug forms for intravenous [13] and intra-arterial delivery [14]. LSCI allows one to obtain complete flow maps in real time without any scanning equipment or contrast agents. It is worth noting, however, that the penetration depth of light is relatively shallow due to restrictions imposed on the penetration of radiation into tissues in the visible spectral range [15]. Therefore, blood flow visualization is feasible only in the near-surface vessels of an organ [16]. At the same time, reliability and low cost [17] are decisive advantages for the widespread use of LSCI [16,18,19].

In the present study, we outline the principle of examination and selection of the optimal dosage regimen of fluorescent microcontainers for targeted arterial administration into kidney vessels via fluorescence tomography and LSCI. Biocompatible capsules obtained by sequential adsorption of polyelectrolytes, which are highly stable [20, 21], may carry drugs [22,23] and labels [{] 24}, and have the capacity for prolonged release of a drug [25], were used as microcontainers. In addition, microcapsules are sufficiently large for mechanical accumulation in small capillaries of the target organ, especially in the case of arterial delivery [26]. However, in contrast to microparticles, they do not have a rigid core and may change their shape to some extent [27], thus ensuring gradual normalization of blood flow if the dosage is chosen correctly [13].

The aim of the present study was to examine the effect of the number of microcapsules and the administered suspension volume on the accumulation of a fluorescent signal in the target kidney by fluorescence tomography and to assess hemodynamic changes in the target organ using LSCI as a method of primary monitoring of critical concentrations leading to irreversible structural changes in the organ.

Materials and methods

Calcium chloride (dihydrate), sodium carbonate (anhydrous), ethylenediaminetetraacetic acid (EDTA) disodium salt, dextran sulfate (DS, MW ¿ 70 000) sodium salt, poly-L-arginine (pArg, MW ¿ 70 000) hydrochloride, rhodamine B isothiocyanate (RITC), phosphate-buffered saline (PBS, 0.1 M), bovine serum albumin (BSA, lyophilized powder), and trypsin from porcine pancreas ($\sim$ 1500 units/mg) were purchased from Sigma-Aldrich (Germany). Hydrochloric acid, dimethyl sulfoxide (DMSO), and cyanine7 NHS ester (Cy7) were provided by „Reakhim“ (Russia), Merck (Germany), and Lumiprobe (Russia), respectively. Trypsin, 1:250, for cell cultures was purchased from MP Biomedicals (United States). All chemical reagents were used without further purification. Deionized water produced using a Milli-Q water purification system (Millipore, United States) was used at all stages of the experiment.

Conjugation of BSA and fluorescent dyes

Solutions of individual components were prepared first. Staining solutions: RITC (7.5 mg) in ethanol (1.5 mL); Cy7 (5 mg) in DMSO (1.5 mL). BSA (60 mg) was dissolved in PBS (13.5 mL). The pH of PBS was adjusted to 8.3 using NaOH solution (1 M). A staining solution (either RITC or Cy7) was added to the BSA solution. This mixture was stirred overnight at 4°C. The fresh conjugate of BSA and a fluorescent dye (either RITC or Cy7) was then dialyzed against deionized water in the dark at 4°C for 3 days.

Synthesis of polyelectrolyte microcapsules

Vaterite ($CaCO_3$) microspheres served as a basis for the formation of microcapsules by the method of layer-by-layer adsorption of oppositely charged polyelectrolytes, which was borrowed, with certain adjustments, from [28]. Vaterite microparticles were obtained by mixing equimolar (0.37 M) solutions of two salts of equal volumes (2 mL): $CaCl_2$ and Na_2CO_3. To incorporate the BSA–Cy7 conjugate into the resulting vaterite matrix, the fluorescent conjugate (2 mg/mL, 0.5 mL) was added to the calcium chloride solution. The resulting mixture was stirred for 1 min. Crystallized microparticles with the incorporated fluorescent BSA–Cy7 conjugate were precipitated by centrifugation at 1000 rcf and rinsed three times with deionized water. Polyelectrolyte layers were formed by cascade adsorption of pArg and DS; each layer was rinsed three times with deionized water. The second layer of dextran sulfate was substituted with BSA–RITC. The formation of layers continued until 3 bilayers were produced. The final shell structure was as follows: pArg/DS/pArg/BSA–RITC/pArg/DS. Vaterite cores were then dissolved in 0.2 M EDTA (pH 7.3) to form hollow microcapsules.

Characterization of fluorescent microcapsules

The morphology of the resulting microcapsules was studied by scanning electron microscopy (SEM) with a MIRA II LMU microscope (TESCAN, Czech Republic) at an operating voltage of 30 kV. A droplet of the microcapsule suspension on a silicon substrate was dried under normal conditions. The samples were then secured to a carbon plate glued to an aluminum sample holder, and vacuum deposition of gold onto the sample surfaces was performed.

The fluorescent properties of fresh microcapsules and their size distribution were studied using a Leica TCS SP8 X inverted confocal microscope fitted with a pulsed white light laser source (the laser power was 1.5 mW) focused through a $20 \times /0.70$ NA objective. The following settings were used: excitation at 554 nm with radiation detection at 570–650 nm (RITC) and excitation at 670 nm with radiation detection at 700–795 nm (Cy7). The size

distribution of microcapsules was estimated by analyzing fluorescence images in the free ImageJ software (i.e., measuring the diameter of 100 microcapsules).

The optical density of solutions of fluorescent conjugates was measured using a microplate reader (Synergy H1, BioTek, United States). The absorption spectrum of solutions was recorded within the 400–850 nm range. Calibration lines were plotted by measuring the optical density of solutions at a single point: 525 nm for BSA–RITC and 762 nm for BSA–Cy7. Figure 1 presents the spectra of fluorescent conjugates and calibration lines calculated by measuring the optical density of solutions with a known concentration of these conjugates.

Subsequent measurements of all supernatants for assessment of the immobilization efficiency and the release kinetics of fluorescent conjugates were carried out at the same settings. The concentrations of conjugates in supernatants were calculated using the calibration lines shown in Fig. 1. Immobilization efficiency was defined as the percentage ratio of the immobilized conjugate mass to the total mass of the conjugate added for incorporation into the carrier:

$$\text{Immobilization efficiency} = \frac{M_{\text{in}} - M_{\text{c-n}}}{M_{\text{in}}} \times 100,$$

where M_{in} is the mass of the fluorescent conjugate added in the process of synthesis of vaterite cores (BSA–Cy7) or formation of layers (BSA–RITC) and $M_{\text{c-n}}$ is the mass of the fluorescent conjugate released into solution at all stages of preparation of microcapsules.

Assessment of the dynamics of release of fluorescent conjugates from microcapsules under the influence of the trypsin enzyme

The dynamics of release of fluorescent conjugates upon coincubation of microcapsules with the trypsin enzyme was examined in accordance with the procedure outlined in [29]. A trypsin solution in PBS with a concentration of 100 μg/mL was prepared. The enzyme solution (200 μL) was added to 100 μL of a suspension of capsules in PBS with a concentration of 10^8 microcapsule/mL. Further incubation was carried out at 37°C and under constant shaking (300 rpm). The incubation of samples was stopped after 5, 15, 30 min, 1, and 3 h. Supernatants were sampled by centrifugation (1000 rcf) and collection of liquid under the sediment. Separate test mixtures were prepared for each time point in triplicate. The optical density of supernatants was measured at a wavelength of 525 nm (BSA–RITC) and 762 nm (BSA–Cy7). The released amount of fluorescent conjugates was calculated in accordance with the calibration lines.

Animal studies

All experimental studies were performed in white male Balb/c mice aged 6–8 weeks (weight, 20–25 g) under general anesthesia (a mixture of Zoletil (40 mg per kg, 50 μL, Virbac SA, Carros, France) and a 2% Rometar solution (10 mg per kg, Spofa, Czech Republic)) by intraperitoneal administration. At the end of the experiment, animals were euthanized by an overdose of anesthesia.

Procedure of intra-arterial administration of microcapsules

Targeted delivery of the suspension of microcapsules to the kidney was performed by implantation of a polyethylene catheter (PE-10, Scientific Commodities INC., Lake Havasu City, Arizona, United States) with a thin polyurethane intravascular tube at the end (40 mm, polyurethane tubing, 32ga/.8Fr, 0.005 × 0.010 inch, Instech, United States) into the left renal artery. The thin section of the saline-filled catheter was implanted through the right femoral artery into the abdominal aorta to the junction of thin and thick sections of the catheter. During this procedure, the positioning of the catheter in the vascular bed was checked by its filling with arterial blood on pulling the piston of a syringe connected to the catheter. The animal was then turned to its right side, and a small incision (8–10 mm) was made on the left side parallel to the spine (2–3 mm away from it) above the kidney. At the next stage, the junction of the left renal artery with the abdominal aorta was found and cleaned of fat and connective tissue with cotton swabs to gain a better view. We then made sure that the catheter was inside the abdominal aorta and its end could be carefully probed with tweezers. Next, the catheter was pulled slightly away from the femoral artery so that its end was positioned in the aorta 3 mm above the junction with the renal artery. After that, the end of the catheter was inserted carefully into the left renal artery. It should be noted that the diameter of the renal artery is slightly larger than the diameter of the catheter, and small quantities of blood may enter the kidney in the course of the above manipulations.

At the last stage, a certain dose (chosen with account for the dead volume of the catheter) of the suspension of capsules was injected into the renal artery. The administration procedure was completed in 10–15 s to ensure uniform distribution of the administered suspension throughout renal vessels. At the moment of injection, one needs to press the walls of the renal artery tightly against the walls of the catheter with tweezers (to avoid penetration of the capsule into the aorta), while also being careful as not to block the lumen of the catheter. A minute after the capsules were administered, the tweezers were removed, the catheter was pulled out carefully from vessels, and the femoral artery was ligated to prevent bleeding. At the end of the operation, the muscle layer and skin were sutured, and a heparin solution was injected 30 min after through the tail vein to avoid thrombosis of the extremities. The procedure of injection into the renal artery was discussed in detail in [30]. Vessels should not be subjected to any strong and prolonged mechanical impact prior to implanting the catheter into the artery. The color and blood supply of

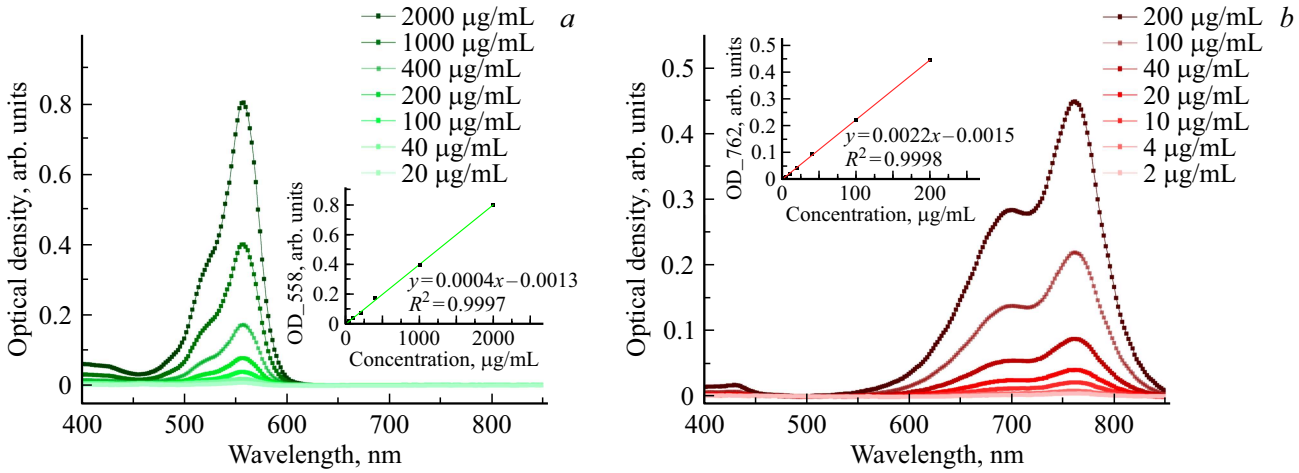

Figure 1. Results of spectrophotometry of fluorescent conjugates: *a* — absorption spectra of BSA–RITC solutions (the calibration line is shown in the inset); *b* — absorption spectra of BSA–Cy7 solutions (the calibration line is shown in the inset).

the kidney should remain normal throughout all stages of the operation up to this point. Only then can the effect of administered drugs and drug containers on renal tissue be assessed correctly.

Biodistribution of microcapsules *in vivo* and *ex vivo*

An IVIS SpectrumCT In Vivo (PerkinElmer, Waltham, MA, United States) imaging system was used to assess the biodistribution of the BSA–Cy7 fluorescent label injected into the renal artery of mice in free form or in microcapsules. Excitation and emission were set to 745 and 800 nm, respectively. Post-processing of the obtained data was performed in Living Image 4.7.3.

At the first stage of research, the number of administered capsules remained unchanged (10^6 microcapsules), and only the administered volume was varied (200, 100, 50, 20, 10 μL) to achieve predominant localization of the fluorescent signal in the target kidney during *in vivo* imaging of the animal lying on its stomach (with its back facing the detectors). The effect of the number of capsules administered ($0.25 \cdot 10^6$, $0.5 \cdot 10^6$, 10^6, $5 \cdot 10^6$, $10 \cdot 10^6$, and $20 \cdot 10^6$ capsules in 10 μL) was examined next. Combined fluorescent images were obtained immediately after the completion of all manipulations (15 min after the introduction of microcapsules) *in vivo* and after killing the animals and dissection of organs (left and right kidneys, liver, lungs, spleen, and heart) for *ex vivo* imaging of the distribution of the fluorescent label associated with microcapsules in the indicated organs.

The total radiant efficiency (TRE) for each organ was measured within its boundaries. The TRE parameter characterizes the total number of photons emitted per second from a chosen area under normalized illumination intensity. The fluorescence percentage for a particular organ was calculated as the ratio of its TRE to the total TRE value for all studied organs of the animal. Pie charts were plotted based on the calculated data on https://piechartmaker.co. When choosing the injection volume, two regions of interest corresponding to the location of the target (left) kidney and liver in the body were analyzed.

Assessment of perfusion of the target (left) kidney by intravital speckle imaging

Changes in blood flow of the left kidney after the introduction of microcapsules were assessed *in vivo* in real time using a proprietary LSCI system. An incision on the back of a mouse made parallel to the spine in the area of the left kidney was freed from surrounding tissue and fixed. Measurements were carried out under general anesthesia directly from the surface of the left kidney prior to the introduction of microcapsules into the renal artery and 15 min, 24 h, and 120 h after it. Data on blood flow were collected after stabilization of hemodynamic parameters. Changes in blood flow were examined in six groups of mice: non-injected animals (control group), animals injected with saline (sham-operated group), and animals injected with a suspension of microcapsules in the following doses: $0.25 \cdot 10^6$, $0.5 \cdot 10^6$, 10^6, $5 \cdot 10^6$, $10 \cdot 10^6$, and $20 \cdot 10^6$ capsules in 10 μL. Blood flow values measured before the injection were taken as baseline ones. These baseline values were determined for each mouse separately. All blood flow measurements were normalized to individual baseline values, and percentage changes were calculated.

A Thorlabs CPS635S laser diode coupled with a Thorlabs DG10-220-MD ground glass diffuser and a Thorlabs LA1131-ML converging lens illuminated uniformly the surface of the target kidney. A Basler a2A2600-64ucBAS digital camera and a Navitar MVL25M1 photo lens were used to capture the subjective speckle pattern. Analyzing the spatial spectrum of the speckle pattern, we adjusted the lens aperture to satisfy the Nyquist criterion. A linear polarizer was mounted in front of the photo lens and

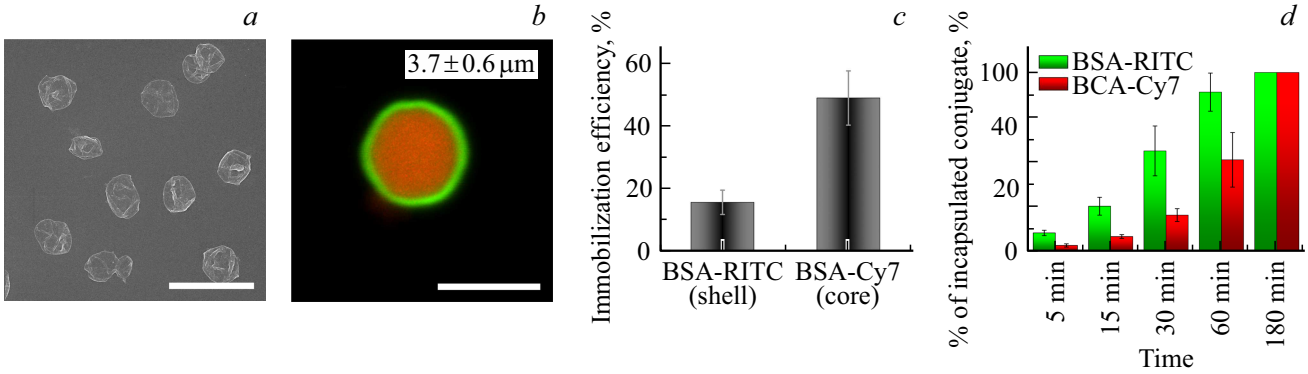

Figure 2. Visualization of microcapsules and the intra-arterial injection scheme. *a* — SEM image of microcapsules made of polyarginine and dextran sulfate (the scale bar is 10 μm). *b* — Fluorescence image of a microcapsule obtained with a Leica TCS SP8 X laser confocal scanning microscope. Red and green colors correspond to the BSA–Cy7 and BSA-RITC conjugates, and the scale bar is 5 μm. The mean diameter and standard deviation calculated using the free ImageJ software based on the measured diameters of 100 microcapsules are shown in the top right corner. *c* — Histogram of the efficiency of immobilization of fluorescent BSA–RITC conjugates into the shell in the process of formation of polyelectrolyte layers and BSA–Cy7 conjugates during the synthesis of vaterite cores. *d* — Dynamics of release of fluorescent conjugates from microcapsules in the course of enzymatic degradation of carriers.

adjusted in such a way as to match the polarization of the laser source. The exposure time and frame rate of the digital camera were set to 10 ms and 30 frames per second, respectively. Custom Python-based software was used to control the LSCI system and process the obtained speckle images. Spatial speckle contrast was calculated as the ratio of the standard deviation of pixel intensity to its mean value in a 5×5 mm sliding window [31]. Averaging over 25 consecutive speckle contrast frames was performed to raise the signal-to-noise ratio in the calculated speckle contrast images. Each blood flow map was smoothed with a Gaussian filter with $\sigma = 7$ in the spatial domain to remove high-frequency fluctuations and highlight coarse changes in the blood flow. A region of interest 200×200 pixels in size was chosen for each data set; the mean and standard deviation were calculated in the chosen region of interest. NumPy v. 1.16.5 and SciPy v. 1.3.1 packages for Python v. 3.6 were used for data processing.

Histological examination of the target (left) kidney

Kidneys were subjected to histological examination 120 h (5 days) after the introduction of microcapsules ($5 \cdot 10^6$ or $20 \cdot 10^6$ capsules in 10 μL of saline) into the left renal artery. Tissue samples were fixed in neutral formalin. The organs were then dried with dehydrated isopropyl alcohol and embedded in paraffin. Slides 5 μm in thickness were stained with hematoxylin and eosin. An Olympus digital image analysis system was used to perform morphological analysis of histological samples.

Results and discussion

The efficiency and safety of delivery of drugs in free or encapsulated form to the kidney through the renal artery depends largely on the correctness of their administration procedure. Every detail, from the speed and accuracy of surgical procedures to the size of carriers used, is of enormous importance. It has been demonstrated earlier [30] that a 29% increase in the size of microcapsules necessitates a 50% reduction in the number of administered capsules if a safe dosage regimen is to be maintained. The advantage of drug delivery systems is the possibility of their mechanical retention due to adhesion to the endothelium of blood vessels and subsequent release of the encapsulated substance [32]. Thus, a source of a therapeutic or biologically active substance forms in the region of interest and stays there until the matrix is degraded completely or swept away from the wall of a blood vessel by blood flow.

Microcapsules made of polyarginine and dextran sulfate with an estimated diameter of 3.7 μm (± 0.6 μm) were used in the present study. Figure 2, *a* shows the image of microcapsules obtained with a scanning electron microscope. The morphology of objects in this image suggests that the microcapsules have a spherical shape and an inner cavity (folds on their surface indicate that the shell, which has a thickness of approximately 50 nm [14] and does not have a solid base, does not retain its shape and collapses when dried). The feasibility of payload immobilization in both the core and the shell of a microcapsule is demonstrated through the primary coprecipitation of a fluorescent conjugate (BSA–Cy7) during the synthesis of vaterite cores and the adsorption of another fluorescent conjugate (BSA–RITC) in the process of layer formation. Fluorescent conjugates do not mix in the prepared capsules and visualize structural elements (the interior and the shell; see Fig. 2, *b*) clearly. The efficiencies (Fig. 2, *c*) and profiles of release upon microcapsule degradation (Fig. 2, *d*) typical of immobilization in the interior and the shell differ, allowing one to use these differences in planning treatment strategies. BSA–Cy7 was used in *in vivo* experiments in the present study as a model macromolecular cargo that may

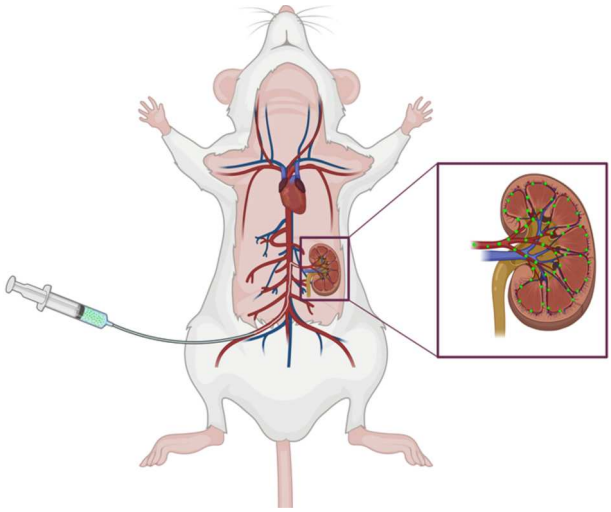

Figure 3. Diagram of catheter implantation through the femoral artery with the aim of reaching the renal artery for subsequent injection of a suspension of microcapsules in saline. The image was generated via Biorender.com.

be localized and visualized by fluorescence tomography, since both excitation and emission wavelengths lie within the optical transparency window of biological tissues.

Microcapsules based on polyarginine and dextran sulfate were used for delivery to the kidney, since they have a number of unique properties: (i) capacity for mechanical deformation due to the lack of a rigid core, which was expected to help maintain normal blood flow in vessels where they would accumulate [33,34]; (ii) extremely low toxicity [35]; (iii) complete biodegradation within a few weeks [36]; and (iv) possibility of functionalization of microcapsule shells with fluorescent agents [37] and nanoparticles [38].

The endovascular method makes it possible to raise locally the concentration of administered substances in the vessels of target organs for both diagnostics [39] and therapy [40]. However, a high concentration of a free therapeutic/diagnostic substance is maintained only for a few seconds. This time interval may be extended through the use of delivery systems, such as microcapsules. However, there is also a risk of embolization: long-term or irreversible blockage of renal vessels, which leads to various complications. Although irreversible embolization is commonly used in experimental nanomedicine and clinical practice before total nephrectomy, it is ill-suited for the treatment of most cases of kidney disease, since normal blood supply and proper functioning of the organ cannot be restored.

Figure 3 shows the diagram of surgical procedures performed to bring the end of a catheter through the femoral artery to the entry of the left renal artery into the target organ (left kidney) for injection of microcapsules directly into the left kidney. At the moment when the suspension of microcapsules has already been introduced but tweezers are still blocking blood flow, the largest number of capsules are found in the vessels of the target kidney and may adhere to the endothelium (while blood flow is obstructed). In clinical practice, standard endovascular catheters with balloons may be used to block blood flow temporarily [41]. In our experiments, blood flow was obstructed for no longer than 1 min. As will be shown below, this made it possible to maintain the normal morphological state of the target kidney tissues. At the last stage of the operation, the catheter was pulled out from the vessels, and organ perfusion was thus restored.

At the first stage of research, the optimum volume of injection into the renal artery was chosen so that *in vivo* visualization of an animal lying on its stomach would reveal predominant localization of the fluorescent agent (BSA–Cy7) in the target organ (Fig. 4). The first tested volume was the injection of 10^6 microcapsules in 200 μL. This volume is close to the upper acceptable limit for intravenous administration performed without adverse effects, such as tachycardia, due to excessive hemodilution [3]. At the same time, it seemed logical that a large volume of injection should be preferable in terms of avoiding irreversible embolization, since a fixed number of microcapsules is distributed more sparsely within a greater volume and the likelihood of blocking a blood vessel with an aggregate of capsules is lower. The IVIS image obtained following the administration of 10^6 capsules in 200 μL of saline demonstrates a clearly dominant distribution of the fluorescent signal in the opposite kidney. A gradual rise of the signal intensity from both kidneys with a reduction in volume is evident in Fig. 4. Presumably, with a large administered volume, a suspension of microcapsules displaces blood not only in the target organ, but also in vessels that are connected or located down the bloodstream, and microcapsules are subsequently distributed throughout the body. Since vessels of the opposite kidney are closest to the target organ, most of the injected microcapsules are likely to pass through them, forming the signal shown in Fig. 4. As the injection volume decreases, fewer and fewer microcapsules leave the target organ, and a minimum value of 10 μL ensures preferential localization of injected microcapsules in the left kidney.

Having determined the optimal injection volume that ensures predominant localization in the target organ in the first minutes after administration, we examined the influence of the number of administered microcapsules on the efficiency of their distribution in the left kidney. It follows from the images presented in Fig. 5, *a* and the histogram in Fig. 5, *c* that the intensity of the detected fluorescent signal (BSA–Cy7) associated with carriers increased in the left kidney area with an increase in the number of introduced microcapsules. The insets in Figs. 5, *a* and *b* reveal the spatial positioning of microcapsules in injected suspensions of the corresponding concentrations. The lowest concentration turned out to be ineffective in terms of adhesion to the endothelium of blood vessels of the left kidney. Thus, in the case of introduction of $0.25 \cdot 10^6$

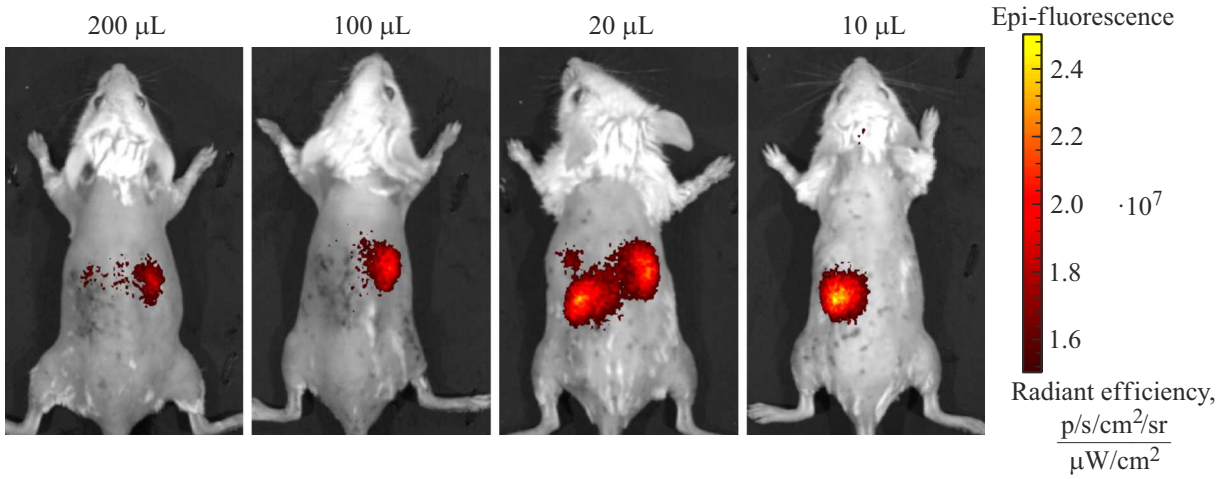

Figure 4. Combined intravital photographic and fluorescent images of animals obtained with an IVIS SpectrumCT In Vivo imaging system 15 min after intra-arterial injection of 10^6 capsules with the fluorescent BSA–Cy7 conjugate in different volumes of saline.

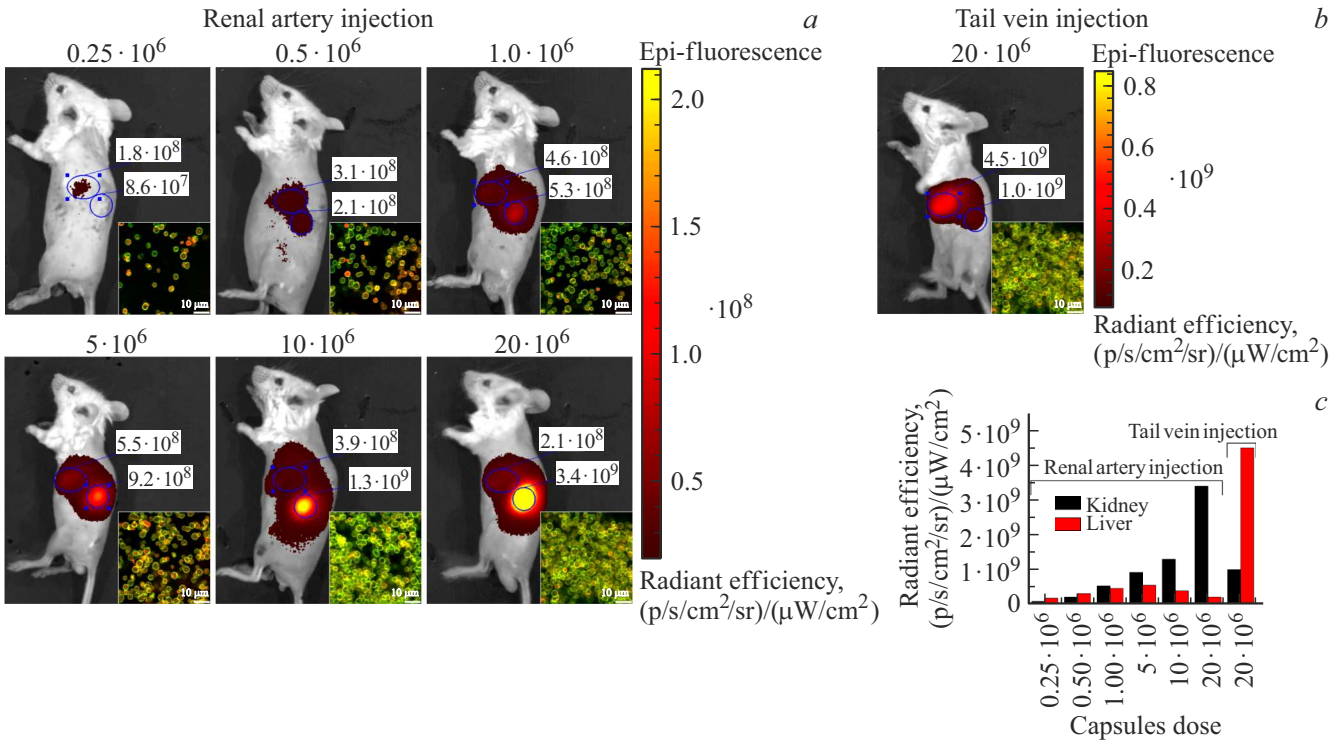

Figure 5. Determination of the number of administered microcapsules that ensures effective accumulation in the target kidney. *a* — Combined intravital photographic and fluorescent images of animals obtained 15 min after intra-arterial administration of $0.25 \cdot 10^6$, $0.5 \cdot 10^6$, 10^6, $5 \cdot 10^6$, $10 \cdot 10^6$, and $20 \cdot 10^6$ capsules in 10 μL of saline. *b* — Combined intravital photographic and fluorescent images of the animal obtained 15 min after intravenous administration of $20 \cdot 10^6$ capsules in 10 μL of saline; TRE values for the liver (the area outlined by the upper oval) and the left kidney (the area outlined by the lower circle) are indicated; fluorescent images of microcapsules in concentrations corresponding to those introduced into animals are shown in the lower right corner (the scale bar is 10 μm). *c* — Histogram of TRE values achieved in the left kidney and liver following the introduction of various doses of microcapsules.

microcapsules, the majority of carriers were swept away and retained in the liver (like all the other micro-sized delivery systems [36]) after the restoration of blood supply to the target organ. As the concentration of microcapsules increased, blood vessels got „packed“ more densely with them. This facilitated the close interaction of a greater number of microcapsules with the inner surface of blood vessels and led to an increase in the likelihood and strength of adhesion, which became so significant that the carriers were able to stay in the left kidney after the restoration of

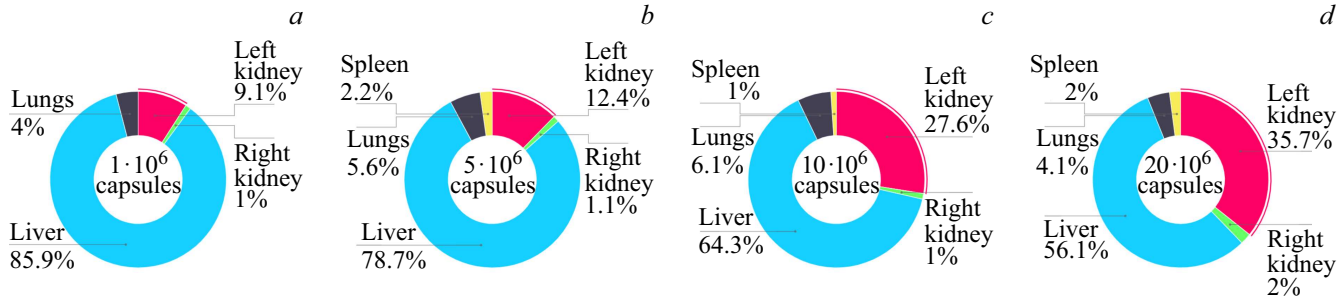

Figure 6. Biodistribution of the fluorescent signal from the BSA–Cy7 conjugate associated with microcapsules determined 15 min after intra-arterial administration of 10^6, $5 \cdot 10^6$, $10 \cdot 10^6$, and $20 \cdot 10^6$ capsules in 10 μL of saline.

blood flow. A comparison of the efficiency of distribution of the fluorescent conjugate in microcapsules upon intra-arterial and intravenous administration revealed that similar TRE values could be obtained with a 4-fold reduction in the administered dose (Fig. 5, *c*). The TRE values achieved after intra-arterial administration of $5 \cdot 10^6$ microcapsules were close to those obtained with intravenous administration of $20 \cdot 10^6$ microcapsules.

An in-depth study of the biodistribution of the fluorescent agent (BSA–Cy7) immobilized into microcapsules was carried out *ex vivo* 15 min after the completion of all surgical procedures; the results of calculation of TRE values of individual organs are presented in Fig. 6. The obtained data verify the validity of above conclusions: (i) the higher the injection concentration is, the greater is the fraction of the administered dose retained in the target organ; (ii) the thinner the administered suspension (low injection concentrations) is, the greater is the amount of microcapsules accumulated in the liver. According to *in vivo* and *ex vivo* fluorescent imaging data, intra-arterial administration of $20 \cdot 10^6$ capsules allows for the most efficient delivery of microcapsules to the left kidney.

A likely mechanism for the accumulation of microcapsules in kidneys is their mechanical entrapment at capillary bends and bifurcations where regions of low blood velocity form. Entering such regions, the capsules slow down and accumulate if the injected suspension has a sufficiently high concentration. This leads to partial (temporary) or complete (irreversible, as will be shown below) occlusion of capillaries. The micrometer size of capsules, which is comparable to the diameter of mice capillaries [42], is an advantage in this case, since it ensures that they get stuck in the first passage through the target organ. This was the explanation provided in [14] for the heavy accumulation of capsules in the glomerular capillary network, which is highly branched and is the first to be encountered along the path of injected capsules. Earlier studies have also demonstrated that the architecture of the vascular bed contributed heavily to the retention of microcapsules in a certain region [33].

The IVIS SpectrumCT In Vivo imaging system allowed us to identify quickly two methodologically important parameters: the injection volume (10 μL) and the number of administered microcapsules ($20 \cdot 10^6$ capsules). However, this research method does not provide an insight into the harm to the target organ. In order to obtain such data, measurements of blood flow of the left kidney of mice were carried out using the LSCI system (Fig. 7) after the introduction of a suspension of microcapsules into the left renal artery in the same doses that were used in *in vivo* experiments on biodistribution (Fig. 5). Data were collected within a certain area (Fig. 7, *b*), since the kidney surface is uniform in structure and the vascular network is isotropic. Data were recorded for each animal prior to injection and 15 min and 24 and 120 h after injection. The results are presented as the difference (normalized to the basal value) between basal blood flow values (before manipulation) and the values determined at a certain time point after administration. To distinguish the effect of introduction of microcapsules from the effect of surgical intervention, two additional groups were formed: a control group (monitoring of blood flow without injection at the same time points with an allowance for an average operation time of 40 min) and a group of sham-operated animals (intra-arterial administration of 10 μL of saline).

A slight (within 20%) change in blood flow detected in the control group is physiologically normal and may be attributed to the influence of anesthesia. The level of blood flow was altered significantly as a result of introduction of microcapsules. The blood flow decreased, on average, by 50% at doses of $0.25 \cdot 10^6$, $0.5 \cdot 10^6$, 10^6, and $5 \cdot 10^6$ microcapsules and by 60–80% at doses of $10 \cdot 10^6$ and $20 \cdot 10^6$ 15 min after injection. A 30–50% reduction in blood flow was also observed in the group of sham-operated animals. This suggests that changes in blood flow with a magnitude below 50% are more likely to be a reaction to the introduction of a certain volume of liquid (10 μL) than to the introduction of capsules and are minimized within just 24 h. However, the experimental groups of animals differed in the nature of change in blood flow observed 24 and 120 h after injection. In the group of animals that received a dose of $0.25 \cdot 10^6$, $0.5 \cdot 10^6$, 10^6, and $5 \cdot 10^6$ microcapsules, the level of blood flow tended to return to the basal value (the detected reduction did not exceed 20% at 24 and 120 h). In the group of animals with a dose of $10 \cdot 10^6$ and $20 \cdot 10^6$ microcapsules, the level of blood flow remained pathologically low (at

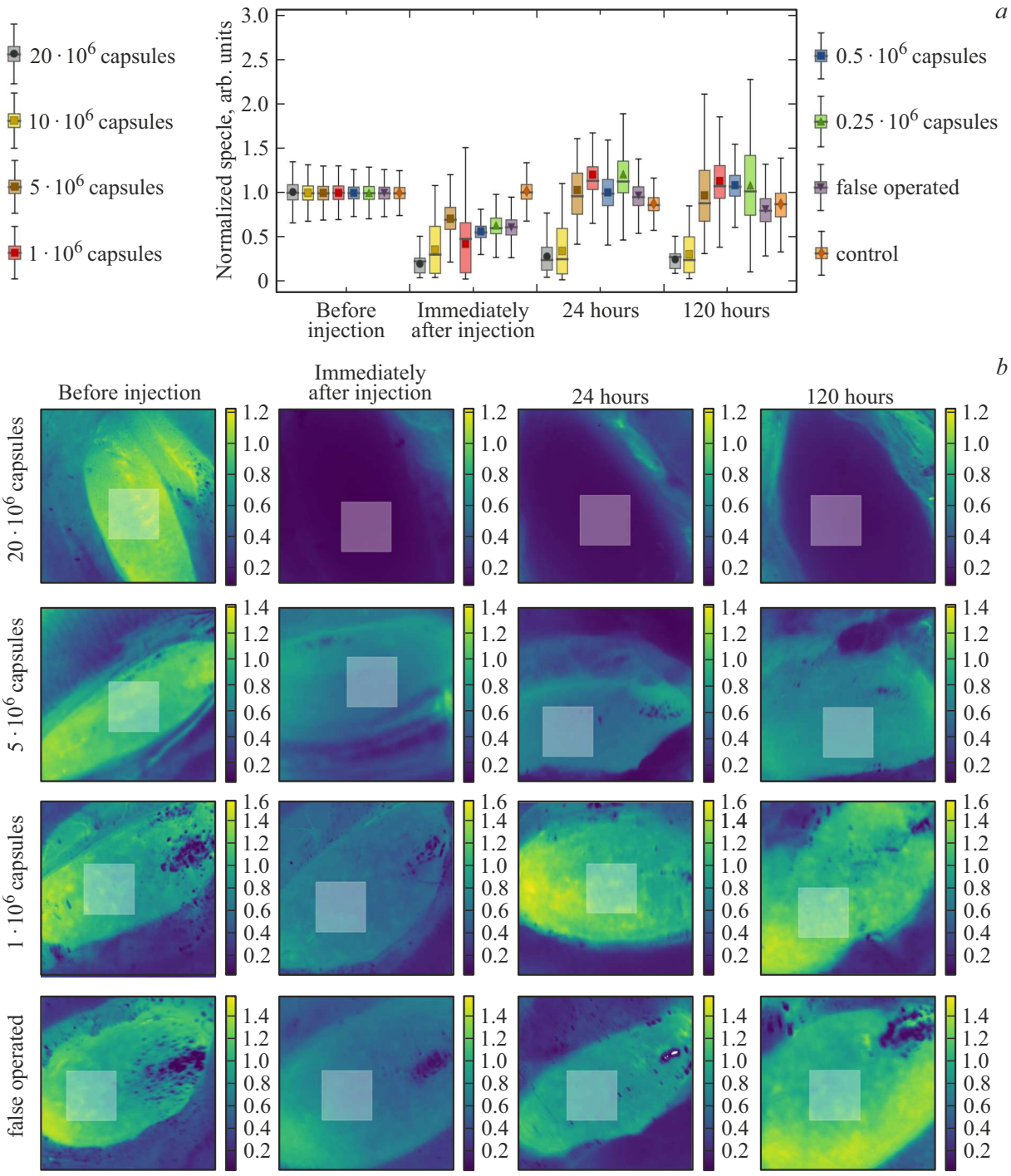

Figure 7. LSCI visualization of changes in blood flow in the target kidney upon administration of various doses of microcapsules. *a* — Results of analysis of speckle patterns of the kidney surface before, immediately after, and 24 and 120 h after intra-arterial injection of various doses of microcapsules and pure saline; the group of non-injected animals was regarded as a control one (with an allowance made for an average operation time of 40 min). *b* — Pseudo-color visualization of the intensity of blood circulation in the near-surface vessels of the organ normalized to the basal level; characteristic speckle patterns from the following groups are presented: sham-operated animals and animals that received an intra-arterial injection of 10^6, $5 \cdot 10^6$, and $20 \cdot 10^6$ microcapsules.

less than 50% of basal values) 24 h and even 120 h after injection. A prolonged temporary occlusion of individual capillaries, which is the likely accompanying effect of the administration of $10 \cdot 10^6$ and $20 \cdot 10^6$ microcapsules, slows down the reperfusion process, as was noted by other research groups [43].

Following removal of the catheter from the artery, blood gradually begins to flow into the kidney, but capsules

in the capillaries prolong this process. This hypothesis was confirmed by a reduction in blood flow detected 15 min after injection (Fig. 7). However, in due course, the capsules are presumably pushed out of the capillaries by blood pressure. As has been demonstrated earlier *in vitro* for tapered glass capillaries [44], this is likely to be attributable to the capacity for mechanical deformation. Capsules displaced by blood enter the efferent arterioles, but their concentration in the tubular capillary network is lower, which reduces the probability of their accumulation and adhesion to the endothelium. Just as in the case of conventional systemic administration, capsules carried by blood flow then spread throughout the systemic circulatory system and accumulate in the liver. However, if the carrier dose is very high, microcapsules irreversibly clog the glomeruli.

Several studies focused on the phenomenon of adhesion to the endothelium of carriers with different sizes, shapes, and rigidity moving in the bloodstream have been published in recent years. Specifically, the authors of [45] have identified the following parameters that influence the adhesion of carriers: the properties of carriers themselves (geometry, density of ligands on the surface, and affinity of ligands for endothelial receptors) and the biophysical properties of the blood vessel wall (endothelial shear rate and density of receptors on the endothelium surface). Thus, certain parameters ensure passive and active adhesion of carriers to the endothelium. Passive adhesion parameters apply to carriers made of any material. The group led by Prof. Paolo Decuzzi has also presented a mathematical model [46] that proves the greater stability of attachment of deformable carriers (e.g., microcapsules) without a rigid core. These effects were examined in the case of normal blood circulation. In the present study, however, we propose a method for introduction of microcapsules that involves complete cessation of blood flow in the target organ for a very short period of time (no more than 90 s) and displacement of the blood itself by a suspension of microcapsules. In accordance with the administration protocol, favorable conditions for adhesion of microcapsules to the endothelium are established within a short time interval. In other words, within approximately 90 s of the introduction of microcapsules, no forces preventing the interaction of these microcapsules with the endothelium remain in action in blood vessels of the kidney. Following removal of the catheter from the renal artery, blood enters the organ again and sweeps away everything that is not bound tightly to the endothelium. It is very important in this technique to find a balance in the number of microcapsules introduced into the target organ, since the greater the amount of injected microcapsules is, the more of them will come into close contact with the blood vessel wall at the first stage (adhesion of carriers to the endothelium). However, at the second stage of operation (restoration of blood flow), an excessive dose of administered capsules induces mechanical clogging of small vessels and their irreversible blockage.

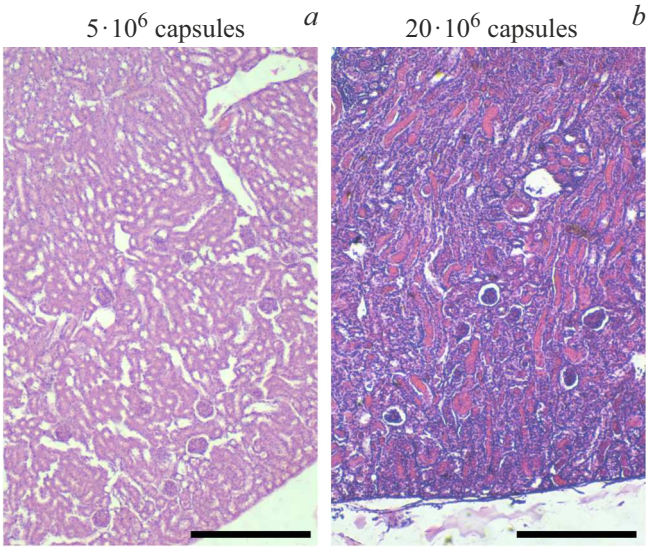

Figure 8. Histological preparations of target kidneys 5 days after intra-arterial administration of (*a*) $5 \cdot 10^6$ and (*b*) $20 \cdot 10^6$ microcapsules. Hematoxylin and eosin staining. The scale bar is 100 μm.

The results of histological examination of tissues of the target organ 5 days after intra-arterial injection (Fig. 8) revealed that normal morphology of all structures of the kidneys of mice having received an injection of no more than $5 \cdot 10^6$ microcapsules was preserved, Signs of impaired blood perfusion, acute ischemia, and necrosis in the left kidney of animals treated with the highest doses ($10 \cdot 10^6$ and $20 \cdot 10^6$ capsules) were observed. Figure 8 shows typical microphotographic images of tissues with undamaged and damaged structures.

Morphological signs of ischemic damage to the left kidney of different severity levels were detected in almost all animals after the injection of $10 \cdot 10^6$ and $20 \cdot 10^6$ capsules. The tubular epithelium was edematous. The outlines and nuclei of nephrocytes were blurred. The lumen of tubules contained cell lysate and red blood cells or was occluded completely. Hyperemia of blood vessels and capillaries was noted in the surviving glomeruli along the periphery of necrosis zones. Bowman's capsules were not dilated uniformly. The capillary glomeruli varied in size, which is likely attributable to the damaged state and swelling of endothelial cells. Focal leukocyte infiltration (demarcation zone), which bounded normal and necrotic areas of the renal tissue, was noted in the stroma. It is important to note that the opposite (right) kidney had an absolutely normal morphological structure. Thus, the results obtained using LSCI were verified by the classical method for identifying pathological processes. The lack of restoration of basal blood flow is indicative of severe damage inflicted by the administration of an excessively large dose of microcapsules.

A dose of $20 \cdot 10^6$ microcapsules, which was determined to be the most effective in fluorescence tomography studies, actually turned out to be unsafe and induced pathological

changes in the target organ. According to the results of LSCI verified by classical histological analysis, a dose of $5 \cdot 10^6$ microcapsules corresponds to the upper safe limit. Thus, $5 \cdot 10^6$ microcapsules in $10\,\mu$L is the actual preferred dosage regimen that ensures the most effective accumulation in the target organ while maintaining the normal state and functioning of this organ.

Conclusion

The use of modern biophotonics methods at the earliest stages of determining the strategy of therapy with novel drug delivery systems allows one to set a correct dosage regimen quickly and accurately and helps avoid undesirable adverse effects induced by ill-chosen parameters of administration of the drug. The advantages of application of the IVIS SpectrumCT In Vivo imaging system for selecting the optimum parameters (volume and concentration) of the administered microcapsule suspension, which ensure effective localization of carriers in the target organ, were demonstrated through the example of targeted delivery of microcapsules to the left kidney of a mouse. The safety of chosen parameters in terms of maintaining normal blood flow was verified rapidly and conveniently by laser speckle contrast imaging. A combination of these two methods may serve as a substitution for the rather lengthy and labor-intensive process of preparation and analysis of histological specimens in screening studies.

Compliance with ethical standards

All experiments with laboratory mice were conducted in accordance with the rules set by the Saratov State Medical University (Ethics Committee protocol No. 7 dated February 02, 2021) and the Geneva Convention of 1985 (International Guiding Principles for Biomedical Research Involving Animals).

Funding

This study was supported financially by the Russian Science Foundation (grant No. 23-75-10070).

Conflict of interest

The authors declare that they have no conflict of interest.

References

[1] A.J. Claxton, J. Cramer, C. Pierce. Clinical therapeutics, **23** (8), 1296–1310 (2001). DOI: 10.1016/S0149-2918(01)80109-0

[2] C. Chen, M. Xie, J. Gong, N. Yu, R. Wei, L. Lei, S. Zhao, R. Li, X. Dong. Frontiers in Pharmacology, **14**, 1132367 (2023). DOI: 10.3389/fphar.2023.1132367

[3] K. Diehl, R. Hull, D. Morton, R. Pfister, Y. Rabemampianina, D. Smith, J. Vidal, C. VanDe Vorstenbosch. Journal of Applied Toxicology: AnInternational Journal, **21** (1), 5–23 (2001). DOI: 10.1002/jat.727

[4] S. Francisco. Journal of pharmaceutical sciences, **75** (9), 852–857 (1986). DOI: 10.1002/jps.2600750906

[5] I. Du, C.T. Ion. Pharmacometrics & Systems Pharmacology, **10** (11), 1276–1280 (2021). DOI: 10.1002/psp4.12701

[6] T. Betz, A. Wunder. Journal of Biomedical Optics, **13** (4), 041311–041311 (2021). DOI: 10.1002/psp4.12701

[7] S. Biffi, C. Garrovo, P. Macor, C. Tripodo, S. Zorzet, E. Secco. Molecular Imaging, **7** (6), 7290 (2008). DOI: 10.2310/7290.2008.00028

[8] M. Novoselova, V. Chernyshev, A. Schulga, E. Konovalova, R. Chuprov-Netochin, T. Abakumova, S. German, V. Shipunova, M. Mokrousov, E. Prikhozhdenko, D. Bratashov, D. Nozdriukhin, A. Bogorodskiy, O. Grishin, S. Kosolobov, B. Khlebtsov, O. Inozemtseva, T. Zatsepin, S. Deyev, D. Gorin. ACS Applied Bio Materials, **5** (6), 2976–2989 (2022). DOI: 10.1021/acsabm.2c00289

[9] Y.W. Jun, H.R. Kim, Y.J. Reo, M. Dai, K.H. Ahn. Chemical science, **8** (11), 7696–7704 (2017). DOI: 10.1039/c7sc03362a

[10] V.V. Tuchin, E.A. Genina, E.S. Tuchina, A.V. Svetlakova, Y.I. Svenskaya. Advanced Drug Delivery Reviews, **180**, 114037 (2022). DOI: 10.1016/j.addr.2021.114037

[11] V.V. Tuchin. *Handbook of coherent-domain optical methods*, 2nd ed. (Springer Science & Business Media, 2013). DOI: 10.1007/978-1-4614-5176-1

[12] D.A. Boas, A.K. Dunn. Journal of biomedical optics, **15** (1), 011109 (2010). DOI: 10.1117/1.3285504

[13] O.A. Sindeeva, R.A. Verkhovskii, A.S. Abdurashitov, D.V. Voronin, O.I.Gusliakova, A.A. Kozlova, O.A. Mayorova, A.V. Ermakov, E.V. Lengert, N.A. Navolokin, V.V. Tuchin, D.A. Gorin, G.B. Sukhorukov, D.N. Bratashov. ACSBiomaterials Science & Engineering, **6** (1), 389–397 (2019). DOI: 10.1021/acsbiomaterials.9b01669

[14] E.S. Prikhozhdenko, O.I. Gusliakova, O.A. Kulikov, O.A. Mayorova, N.A. Shushunova, A.S. Abdurashitov, D.N. Bratashov, N.A. Pyataev, V.V. Tuchin, D.A. Gorin, G.B. Sukhorukov, O.A. Sindeeva. Journal of controlled release, **329**, 175–190 (2021). DOI: 10.1016/j.jconrel.2020.11.051

[15] M.A. Davis, S.S. Kazmi, A.K. Dunn. Journal of biomedical optics, **19** (8), 086001–086001 (2014). DOI: 10.1117/1.JBO.19.8.086001

[16] J. Senarathna, S. Member, A. Rege, N. Li, N.V. Thakor. IEEE Reviews inBiomedical Engineering, **6**, 99–110 (2013). DOI: 10.1109/RBME.2013.2243140

[17] L.M. Richards, S.M.S. Kazmi, J.L. Davis, K.E. Olin, A.K. Dunn. Biomedical optics express, **4** (10), 2269–2283 (2013). DOI: 10.1364/BOE.4.002269

[18] C. Linkous, A.D. Pagan, C. Shope, L. Andrews, A. Snyder, T. Ye, M. Valdebran. JID Innovations, **3** (5), 100187 (2023). DOI: 10.1016/j.xjidi.2023.100187

[19] W. Heeman, E.C. Boerma, W. Heeman, W. Steenbergen, G.M. Van Dam, E.C. Boerma. Journal of biomedical optics, **24** (8), 080901 (2019). DOI: 10.1117/1.JBO.24.8.080901

[20] A.V. Ermakov, R.A. Verkhovskii, I.V. Babushkina, D.B. Trushina, O.A. Inozemtseva, E.A. Lukyanets, V.J. Ulyanov, D.A. Gorin, S. Belyakov, M.N. Antipina. Pharmaceutics, **12** (7), 610 (2020). DOI: 10.3390/pharmaceutics12070610

[21] O.A. Inozemtseva, D.V. Voronin, A.V. Petrov, V.V. Petrov, S.A. Lapin, A.A. Kozlova. Colloid Journal, **80**, 771–782 (2018). DOI: 10.1134/S1061933X19010071
[22] P.A. Demina, A.A. Abalymov, D.V. Voronin, A.V. Sadovnikov, M.V. Lomova. Materials Chemistry Frontiers, **5** (5), 2007–2018 (2021). DOI: 10.1039/d0qm00732c
[23] N.A. Shushunova, O.A. Mayorova, E.S. Prikhozhdenko, O.A. Goryacheva, O.A. Kulikov, V.O. Plastun, O.I. Gusliakova, A.R. Muslimov, O.A. Inozemtseva, N.A. Pyataev, A.A. Shirokov, D.A. Gorin, G.B. Sukhorukov, O.A. Sindeeva. International Journal of Molecular Sciences, **24** (3), 2784 (2023). DOI: 10.3390/ijms24032784
[24] Y. Svenskaya, F. Garello, E. Lengert, A. Kozlova, R. Verkhovskii, V. Bitonto, M.R. Ruggiero, S. German, D. Gorin, E. Terreno. Nanotheranostics, **5** (3), 362 (2021). DOI: 10.7150/ntno.59458
[25] O. Kopach, K. Zheng, L. Dong, A. Sapelkin, N. Voitenko, G. Sukhorukov, D.A. Rusakov. Drug Delivery, **25** (1), 435–447 (2018). DOI: 10.1080/10717544.2018.1431981
[26] O.A. Mayorova, O.A. Sindeeva, M.V. Lomova, O.I. Gusliakova, Y.V. Tarakanchikova, E.V. Tyutyaev, S.I. Pinyaev, O.A. Kulikov, S.V. German, N.A. Pyataev, D.A. Gorin, G.B. Sukhorukov. Nanomedicine: Nanotechnology, Biology, and Medicine, **28**, 102184 (2020). DOI: 10.1016/j.nano.2020.102184
[27] A. Fery, R. Weinkamer. Polymer, **48** (25), 7221–7235 (2007). DOI: 10.1016/j.polymer.2007.07.050
[28] D.V. Volodkin, N.I. Larionova, G.B. Sukhorukov. Biomacromolecules, **5** (5), 1962–1972 (2004). DOI: 10.1021/bm049669e
[29] M.V. Lomova, A.I. Brichkina, M.V. Kiryukhin, E.N. Vasina, A.M. Pavlov, D.A. Gorin, G.B. Sukhorukov, M.N. Antipina. ACS applied materials & interfaces, **7** (22), 11732–11740 (2015). DOI: 10.1021/acsami.5b03263
[30] O.I. Gusliakova, E.S. Prikhozhdenko, V.O. Plastun, O.A. Mayorova, N.A. Shushunova, A.S. Abdurashitov, O.A. Kulikov, M.A. Abakumov, D.A. Gorin, G.B. Sukhorukov, O.A. Sindeeva. Pharmaceutics, **14** (5), 1056 (2022). DOI: 10.3390/pharmaceutics14051056
[31] D.D. Duncan, S.J. Kirkpatrick, M. Larsson, T. Stromberg, O.B. Thompson. Journal of biomedical optics, **18** (6), 066018–066018 (2023). DOI: 10.1117/1.JBO.18.6.066018
[32] B.V. Parakhonskiy, N.Y. Shilyagina, O.I. Gusliakova, A.B. Volovetskiy, A.B. Kostyuk, I.V. Balalaeva, L.G. Klapshina, S.A. Lermontova, V. Tolmachev, A. Orlova, D.A. Gorin, G.B. Sukhorukov, A.V. Zvyagin. Applied MaterialsToday, **25**, 101199 (2021). DOI: 10.1016/j.apmt.2021.101199
[33] D.V. Voronin, O.A. Sindeeva, M.A. Kurochkin, O.A. Mayorova, I.V. Fedosov, O.V. Semyachkina-Glushkovskaya, D.A. Gorin, V.V. Tuchin, G.B. Sukhorukov. ACS Applied Materials & Interfaces, **9** (8), 6885–6893 (2017). DOI: 10.1021/acsami.6b15811
[34] A.A. Abdurashitov, E.S. Prikhozhdenko, O.A. Mayorova, P.O. Plastun, O.I. Gusliakova, N.S. Shushunova, O.A. Kulikov, V.V. Tuchin, G.B. Sukhorukov, O.A. Sindeeva. Biomedical optics express, **12** (7), 4467–4477 (2021). DOI: 10.1364/BOE.430393
[35] D.B. Trushina, R.A. Akasov, A.V. Khovankina, T.N. Borodina, T.V. Bukreeva, E.A. Markvicheva. Journal of molecular liquids, **284**, 215–224 (2019). DOI: 10.1016/j.molliq.2019.03.152
[36] N.A. Navolokin, S.V. German, A.B. Bucharskaya, O.S. Godage, V.V. Zuev, G.N. Maslyakova, N.A. Pyataev, P.S. Zamyshliaev, M.N. Zharkov, G. STerentyuk, D.A. Gorin, G.B. Sukhorukov. Nanomaterials, **8** (10), 1–14 (2018). DOI: 10.3390/nano8100812
[37] P.A. Demina, O.A. Sindeeva, A.M. Abramova, E.S. Prikhozhdenko, R.A. Verkhovskii, E.V. Lengert, A.V. Sapelkin, I.Y. Goryacheva, G.B. Sukhorukov. ACS Applied Materials & Interfaces, **13** (17), 19701–19709 (2021). DOI: 10.1021/acsami.1c02767
[38] I.A. Burmistrov, M.M. Veselov, A.V. Mikheev, T.N. Borodina, T.V. Bukreeva, M.A. Chuev, S.S. Starchikov, I.S. Lyubutin, V.V. Artemov, D.N. Khmelenin, N.L. Klyachko, D.B. Trushina. Pharmaceutics, **14** (1), 65 (2021). DOI: 10.3390/pharmaceutics14010065
[39] J. Miller, D. Edward, P. Ruben, A. Nelson, D. Luers, A. Sherry, F.P. Lawrence, E. Anderson, A. Kruger. Radiology, **148** (1), 273–278 (1983). DOI: 10.1148/radiology.148.1.6407063
[40] X.I.P. Doulamis, A. Guariento, T. Duignan, T. Kido, A. Orfany, M.Y. Saeed, V.H. Weixler, D. Blitzer, B. Shin, E.R. Snay, J.A. Inkster, A.B. Packard, D. Zurakowski, T. Rousselle, A. Bajwa, S.M. Parikh, I.E. Stillman, P.J. Nido, J.D. Mccully. American Journal of Physiology. Renal Physiology, **319** (3), 403–413 (2020). DOI: 10.1152/ajprenal.00255.2020
[41] B. Tesfamariam. Journal of Controlled Release, **238**, 149–156 (2016). DOI: 10.1016/j.jconrel.2016.07.041
[42] S. Lang, M. Dominietto, M. Rudin, G. Schulz, H. Deyhle, M. Germann, F. Pfeiffer, C. David, T. Weitkamp. Proceedings Developments in X-RayTomography VI, **7078**, 89–98 (2008). DOI: 10.1117/12.794157
[43] D.N. Granger, P.R. Kvietys. Redox Biology, **6**, 524–551 (2015). DOI: 10.1016/j.redox.2015.08.020
[44] S. She, C. Xu, X. Yin, W. Tong, C. Gao. Langmuir, **28** (11), 5010–5016 (2012). DOI: 10.1021/la3003299
[45] A.L. Van De Ven, P. Kim, O.H. Haley, J.R. Fakhoury, G. Adriani, J. Schmulen, P. Moloney, F. Hussain, M. Ferrari, X. Liu, S. Yun, P. Decuzzi. Journal of Controlled Release, **158** (1), 148–155 (2012). DOI: 10.1016/j.jconrel.2011.10.021
[46] A. Coclite, G. Pascazio, M.D. De Tullio, P. Decuzzi. Journal of Fluidsand Structures, **82**, 638–650 (2018). DOI: 10.1016/j.jfluidstructs.2018.08.001

Translated by D.Safin